An Integrated Study on the Evolution of Inclusions in EH36 Shipbuilding Steel with Mg Addition: From Casting to Welding

XIAODONG ZOU, DAPENG ZHAO, JINCHENG SUN, CONG WANG, and HIROYUKI MATSUURA

Inclusion evolution behaviors, in terms of composition, size, and number density, and associated influence on the microstructures of the as-cast slabs, rolled plates, and simulated welded samples of plain EH36 and EH36-Mg shipbuilding steels have been systematically investigated. The results indicate that the inclusions in the as-cast plain EH36 are almost Al-Ca-S-O-(Mn) complex oxides with sizes ranging from 1.0 to 2.0 μm. After Mg addition, a large amount of individually fine MnS precipitates and Mg-containing Ti-Al-Mg-O-(Mn-S) complex inclusions are generated, which significantly refine the microstructure and are conducive to the nucleation of acicular ferrite in the rolled and welded sample. Moreover, after rolling and welding thermal simulation, the number of individual MnS decreases gradually due to its precipitation on the surface of Ti-Al-Mg-O oxides.

https://doi.org/10.1007/s11663-017-1163-x

I. INTRODUCTION

DURING steelmaking and casting, non-metallic inclusions are inevitably generated due to active elements in steel contacting and reacting with refractory materials and slags. In addition, impurity elements in the solidification process will also incur segregation and secondary reactions to generate inclusions. According to traditional views and experiences, inclusions are harmful to steel properties such as toughness, fatigue, and strength.[1,2] Therefore, various attempts have been exercised to remove inclusions in steels. However, with improved understanding of inclusions, particularly their positive influences on steel microstructures, it generally comes to a consensus to enable full utilization of particular groups of inclusions during pertinent metallurgical processes, which is coined as Oxide Metallurgy.[3]

Recently, high heat input welding has gained engineering significance for improving welding efficiency and lowering construction cost.[4] However, high heat input welding usually involves longer residence at high temperature and lower cooling rate, which invariably leads to significant coarsening of austenite grains and formation of brittle microstructures such as ferrite side plate (FSP), upper bainite (Bu), and coarsening grain boundary ferrite (GBF), resulting in the reduced toughness of Heat-Affected Zone (HAZ).[5,6] Therefore, it is imperative to investigate alternative techniques that can uphold high heat input welding while keeping the outstanding issues minimal.

For low-carbon low alloy steels, numerous researchers have successfully mated the concept of Oxide Metallurgy to high heat input welding. Many researchers found that certain types of fine oxide inclusions with high melting points could increase the toughness and strength of HAZ.[7–9] The inclusions could pin the austenite grain boundaries for grain refinement of ferrite.[10] Meanwhile, the process of nucleation on the inclusions leads to a chaotic arrangement of laths and a fine-grained interlocking microstructural characteristics of acicular ferrite (AF).[11] In general, a microstructure consisting primarily of AF provides optimum HAZ mechanical properties.[12,13] One proven way to control non-metallic inclusions and improve microstructure is the utilization of specific additives with strong affinities to O and S such as Mg, Ti, and Zr.[14] For instance, Xu *et al.*[15] articulated the effect of Mg content on the microstructure and toughness of HAZ of EH36 shipbuilding steel plate after high heat input welding, and found that with the increase of Mg content major microstructural constituents in HAZ changed from the GBF, FSP, and Bu to AF. Meanwhile, Zhu *et al.*[16] found that the toughness of HAZ was improved

XIAODONG ZOU, DAPENG ZHAO, JINCHENG SUN, and CONG WANG are with the School of Metallurgy, Northeastern University, Shenyang 110819, China. Contact e-mail: wangc@smm.neu.edu.cn HIROYUKI MATSUURA is with the Department of Materials Engineering, The University of Tokyo, Tokyo 113-8656, Japan.

Manuscript submitted August 15, 2017.
Article published online December 27, 2017.

significantly by adding 50 ppm Mg to Ti-bearing low-carbon steels and austenite grain growth was inhibited by the formation of pining particles after the addition of Mg. Wu *et al.*[17] investigated the effect of the precipitation behavior of beneficial inclusions on the microstructure in both as-cast and hot-rolled Al-Ti deoxidized and Mg-treated steel. Suito *et al.*[8] reported the influence of oxide particles and residual elements on microstructure and toughness in the HAZ of low-carbon steel deoxidized with Ti and Zr.

Although tremendous efforts have been documented, few studies harnessing the integrated understanding of each step of the steel manufacturing chain, including steelmaking, casting, rolling as well as welding, on the evolution of inclusions and microstructures, are available. EH36 steel, one of the typical high-performance low alloy steels, is required to possess better properties such as high strength, good toughness, and excellent welding properties[18] and is chosen as the target steel. In this paper, we present a rather holistic and unique view featuring inclusion evolution characteristics, namely, composition, morphology, size, and number density, of the Mg-treated EH36 shipbuilding steel, after notable checking points, such as casting, rolling as well as high heat input welding. Concurrent to inclusion features, ensuing microstructures and mechanical properties are characterized to offer quantitative explanations and derive mechanisms governing end user performances.

II. EXPERIMENTAL

Chemical compositions of the targeted steels, namely, plain EH36 and EH36-Mg are shown in Table I. Both alloys were treated by Ti-Al deoxidation, while the latter one was further processed with 7 ppm Mg addition in the form of Mg-Ni alloy (29.72 mass pct Mg, 70.03 mass pct Ni). After casting, thermo-mechanically controlled processing (TMCP, Figure 1) was introduced into the production of steel plate for improving the weldability and workability. Cast steel ingots were reheated in a temperature of about 1473 K (1200 °C), and hot rolled into plates of 60 mm in thickness by a rolling mill with a finish rolling temperature of 1113 K (840 °C).

To simulate welding, samples with a size of 10 × 10 × 80 mm^3 from both rolled steels were prepared for HAZ simulation on a Gleeble 3800 machine. The peak temperature was set at 1673 K (1400 °C) with a dwell time of 3 second. Targeted heat input was estimated to be 120 kJ/cm with a heating rate of 150 K/s. Thermal cycles were described by employing the Rykalin-2D heat transfer model.

All as-cast, rolled, and welding thermal simulation steel samples were prepared in the sequence of cutting, grinding, and polishing. The morphology, composition size, and number of the inclusions in the samples were analyzed by a field emission scanning electron microscope (FE-SEM, Model: Hitachi SU8010) with energy dispersive spectrometer (EDS). Only inclusions confirmed by EDS analysis (respective atomic percentage > 1) were selected and taken into account for statistical significance. To calculate the number density of inclusions, each sample was observed by using SEM-EDS combined method under ×5000 magnification, by which the information of inclusions in specific area of 0.5 × 0.5 mm^2 were recorded. The microstructure in all samples etched by a 4 pct nital solution was observed by optical microscope (OM, Model: Zeiss Axio Imager M2m). To investigate the effects of inclusions on mechanical properties, standard samples from as-cast and rolled steel samples were machined for tensile tests and samples from rolled steels with a size of 10 × 10 × 55 mm^3 were machined for Charpy impact tests at 233 K (− 40 °C), respectively.

III. RESULTS

A. *Evolution of Inclusions*

1. *Evolution of inclusions in plain EH36*

The morphology and composition of typical inclusions in the as-cast plain EH36 sample are shown in Figures 2(a) and (b) (inclusions compositions are in atomic percentage, similarly here in after). As can be seen, inclusions are almost Al-Ca-S-O-(Mn) complex oxides and individual MnS precipitates. The formation of Al-Ca-S-O complex inclusions is due to liquid Al_2O_3-CaO inclusions reaction with the dissolved S, resulting in CaS precipitation during solidification.[19] Typical inclusions in the rolled EH36 sample are presented in Figures 2(c) and (d), which are mainly Al-Ca-S-O-Mn, O-Ca-Mn-S-(Ti-Si), and individual MnS. It can be seen that TMCP resulted in appreciable alteration of inclusion compositions, namely, Al and Ca contents increase slightly in Al-Ca-S-O-(Mn) complex inclusions. Representative examples of inclusions in the sample after welding thermal simulation experiments are presented in Figures 2(e) and (f). The morphology and composition of inclusions remain largely unchanged, though inclusion size grows, the details of which will be discussed in later sections.

The evolution of number and size distribution of inclusions in plain EH36 samples are shown in Figure 3. The number density of the inclusions in plain as-cast EH36 sample is 44 N/mm^2, and their average size is

Table I. Chemical Compositions of Plain EH36 and EH36-Mg Steel Samples (Weight Percent)

Samples	C	Si	Mn	Ni	Al	B	V	Nb	N	Mg	O	S	Ti
EH36	0.053	0.21	1.18	0.12	0.037	< 0.0005	< 0.01	0.012	0.0026	—	0.0010	0.003	0.015
EH36-Mg	0.052	0.15	1.53	0.36	0.0065	0.0008	0.014	0.014	0.0027	0.0007	0.0019	0.004	0.010

1.576 μm. The size of inclusions mainly lies in the range of 1.0 to 2.0 μm. After TMCP, the number and size distribution of inclusions in EH36 undergo appreciable change. The number density and average size turn into 108 N/mm^2 and 2.003 μm, respectively. The increase of number density may be attributed to secondary oxidation by oxygen in air and to form new inclusions, and inclusion growth due to holding at 1473 K (1200 °C) for 2 hours during rolling. The size of inclusions in plain EH36 mostly ranges from 1.0 to 5.0 μm. After welding thermal simulation, the number of inclusions decreases to 48 N/mm^2 and the size distribution of inclusions has a significant change that the number of inclusions decreased, especially for inclusions less than 0.5 μm. During welding simulation, high temperature may likely prevent the formation of MnS due to changed solubility of Mn and S, which leads to less MnS formation and reduced number density.

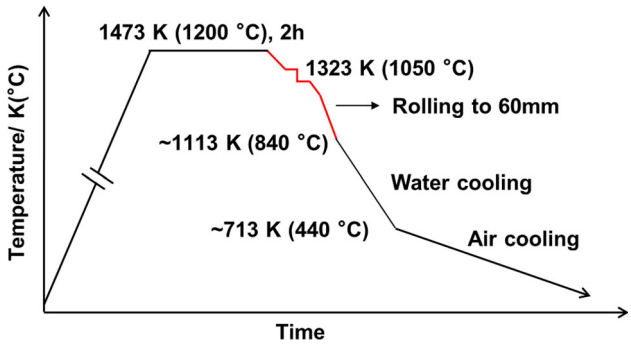

Fig. 1—Temperature profile of TMCP.

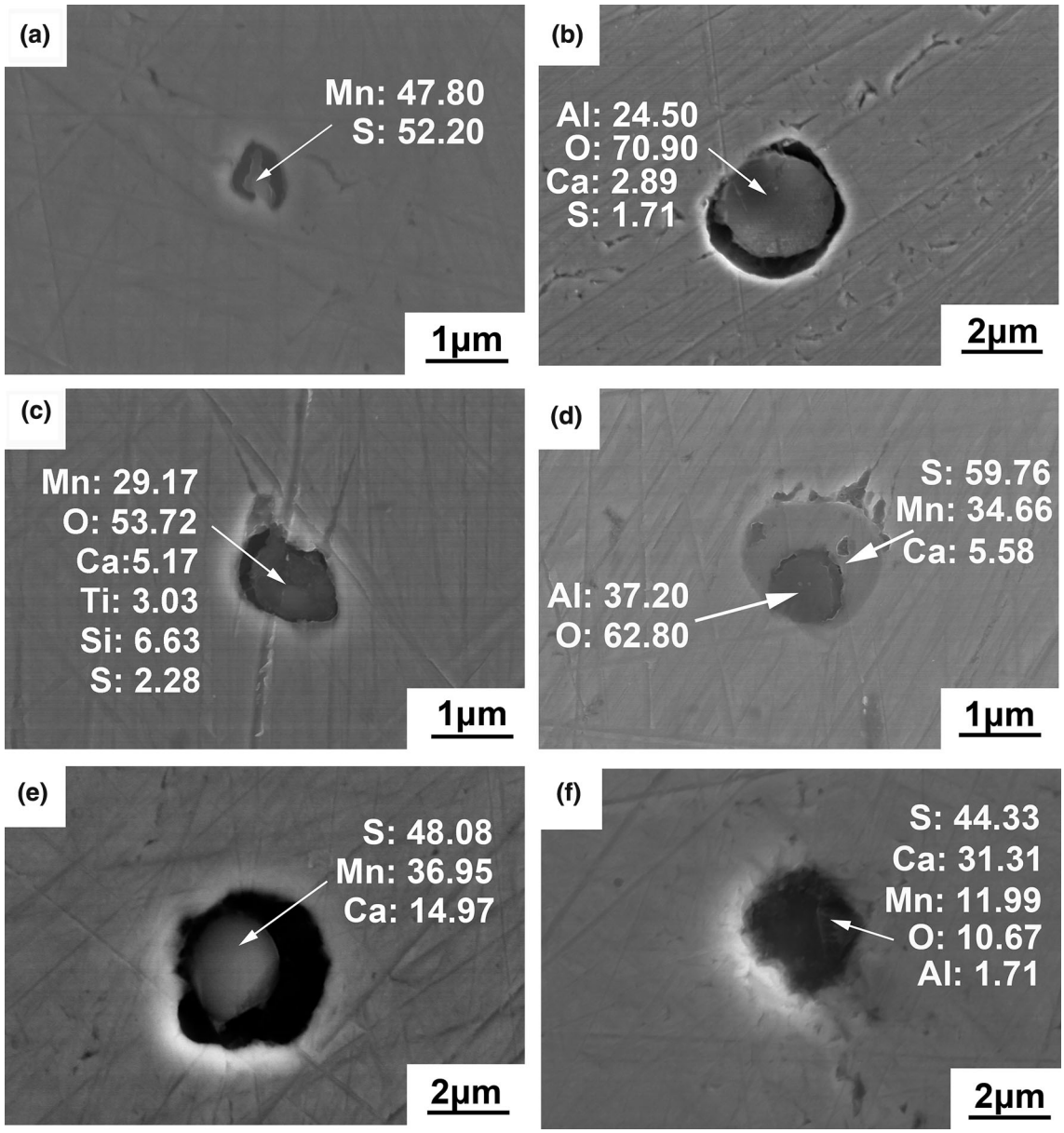

Fig. 2—Morphology and composition of typical inclusions in the (*a*), (*b*) as-cast, (*c*), (*d*) as-rolled, and (*e*), (*f*) as-welded samples of plain EH36.

2. *Evolution of inclusions in EH36-Mg*

Documented studies reported that Mg additions will lead to the change of inclusions' characteristics. The compositional change of inclusions with the addition of Mg in the as-cast sample is presented in Figures 4(a) and (b). The SEM and EDS results indicate that a large amount of individually fine MnS precipitates and Mg-containing Ti-Al-Mg-O-(Mn-S) complex oxides are generated. It is suggested that with Mg addition, Mg-containing complex inclusions are generated, but no individual MgO. Chai *et al.*[20] reported that the evolution of the inclusions in the steels with Mg treatment in Ti-Mg deoxidized steel was in the order of TiO_x, TiO_x mixed with Ti-Mg-O, Ti-Mg-O mixed with MgO, and individual MgO, which is produced with a high content of Mg (about 60 ppm). In the rolled sample, the number of individual MnS precipitation decreases and most of Mn and S precipitate on the surface of complex inclusions, as shown in Figures 4(c) and (d). After welding thermal simulation, the inclusions in EH36-Mg are almost multilayer or mosaic structure, consisting of Ti-Al-Mg-O complex oxides in core and MnS on the surface as shown in Figures 4(e) and (f). The shape of Ti-Al-Mg-O oxides is mostly spherical. From the above observation, it can be concluded that the Ti-Al-Mg-O oxide catalyzes MnS precipitation on the surface, which is consistent with the findings by Wu *et al.*,[17] who also considered that Mg treatment in Al-Ti deoxidized steel was effective to reduce the possibility of individual MnS precipitation. Therefore, individual MnS is hardly found in the above observed EH36-Mg sample.

Figure 5 shows the evolution of number and size distribution of the inclusions in EH36-Mg samples. The number densities of the inclusions in as-cast, rolled, and welded EH36-Mg are 328, 220, and 40 N/mm^2, and their average size are 0.7, 0.653, and 2.326 μm, respectively. It can be seen that comparing with plain EH36, the number of inclusions, especially those sizes < 1 μm, in as-cast EH36-Mg, increases substantially. After rolling, fine MnS precipitates largely disappear and the size of inclusions in EH36-Mg does not change much like that in EH36. Ohta and Suito[21] reported that Mg-containing inclusions in Fe-10 wt pct Ni alloy grew slowly comparing with that of Mg-free. After welding thermal cycle, the size distribution of inclusions in EH36-Mg has a significant change that the number of inclusions between 2 and 5 μm increases and that of less than 1 μm disappears.

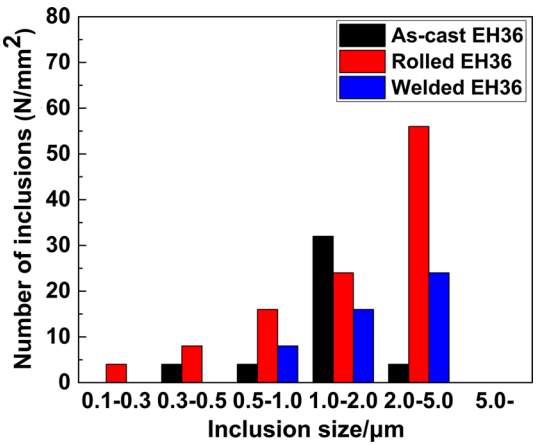

Fig. 3—Number and size distribution of inclusions in plain EH36.

B. *Evolution of Microstructures*

The evolution of microstructure observed by OM in plain EH36 is shown in Figure 6. The microstructure in the as-cast EH36 sample is composed of polygonal ferrite (PF) and pearlite (P) as shown in Figure 6(a). Mukunthan *et al.*[22] found similar microstructure constituents of PF and P at a low cooling rate of 0.1 K/s through austenite transformation in a low-carbon steel strip casting sample. After rolling, grains were significantly refined from 73.87 to 21.10 μm, as shown in Figure 6(b). After welding thermal simulation, austenite grains are coarsened and significant amounts of GBF, FSP, and Bu are generated.

Figure 7 shows the evolution of microstructure in EH36-Mg samples. It can be seen that the microstructure of as-cast EH36-Mg (Figure 7(a)) is also composed of PF and P. However, it is noticeable that Mg addition significantly refines grain sizes from 73.87 to 34.58 μm comparing with plain EH36. The result indicates that the Mg-containing inclusions effectively pin the austenite grain boundary and inhibit the growth of grains.[16] The microstructure of the as-rolled sample mainly consists of dominant AF and PF, as shown in Figure 7(b). The nucleation of AF indicates Mg addition generates effective nucleation sites for AF. Figure 7(c) shows the microstructure of the EH36-Mg steel after welding thermal simulation. The microstructures are composed of salient AF and some GBF, FSP, and Bu features. Comparing with plain EH36 steel, the area fraction of GBF is much smaller in EH36-Mg samples. The Ti-Al-Mg-O inclusions introduced by Mg addition likely induce the nucleation of interlocking AF during $\gamma \rightarrow \alpha$ phase transformation, which can refine the grains and effectively inhibit the expansion of the crack and inhibit the formation of GBF, FSP, and Bu at the same time.[15]

Samples of rolled and welded EH36-Mg are observed by SEM-EDS, and AFs nucleated on typical inclusions are shown in Figures 8 and 9, respectively. It can be found that AFs nucleate on the surface of Ti-Al-Mg-O-Mn-S complex inclusion, whose composition in inner layer is mainly Al_2O_3-MgO spinel.

In order to compare the change of mechanical properties after Mg addition in EH36, tensile tests were carried out for both as-cast and rolled samples and the result is shown in Table II. The yield strength of as-cast EH36 and EH36-Mg are 238 and 264 MPa, and the tensile strength are 380 and 411 MPa, respectively. The yield strength of rolled EH36 and EH36-Mg are 390 and 415 MPa, and the tensile strength are 489 and 531 MPa, respectively. It can be seen that the strength of EH36-Mg is higher than that of plain EH36 due to the refinement of grains by Mg-containing inclusions as shown in Figures 6 and 7.

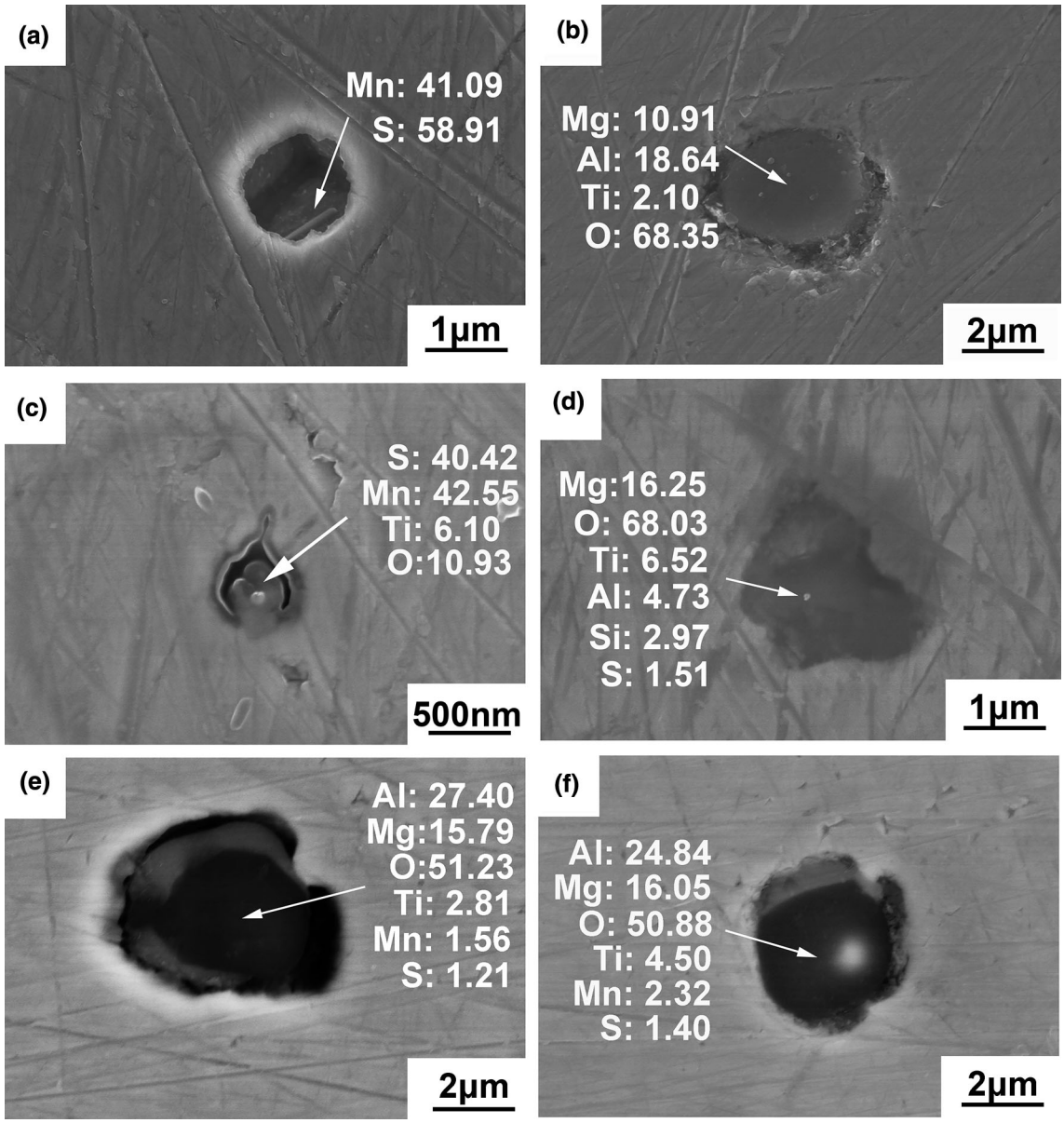

Fig. 4—Morphology and composition of typical inclusions in the (*a*), (*b*) as-cast, (*c*), (*d*) as-rolled, and (*e*), (*f*) as-welded samples of EH36-Mg.

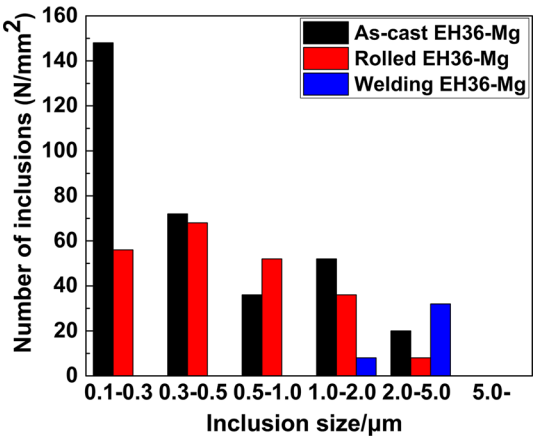

Fig. 5—Number and size distribution of inclusions in EH36-Mg.

Subsequent to tensile tests, Charpy impact tests were carried out for rolled samples. The results are shown in Table III. The impact toughness at 233 K (− 40 °C) of rolled EH36 and EH36-Mg are 265 and 322 J, respectively. It is indicated that the formation of AF induced by Mg-containing inclusions is conducive to improve toughness.

IV. DISCUSSION

A. *Individual MnS Precipitation in EH36-Mg*

It is shown in Figures 4 and 5 that with Mg addition, a large amount of individually fine MnS precipitate in the as-cast sample. Sakata *et al.*[23] studied the effect of Mg deoxidation on the solidification structure in Fe-10 mass pct Ni alloy. They found that columnar dendrites

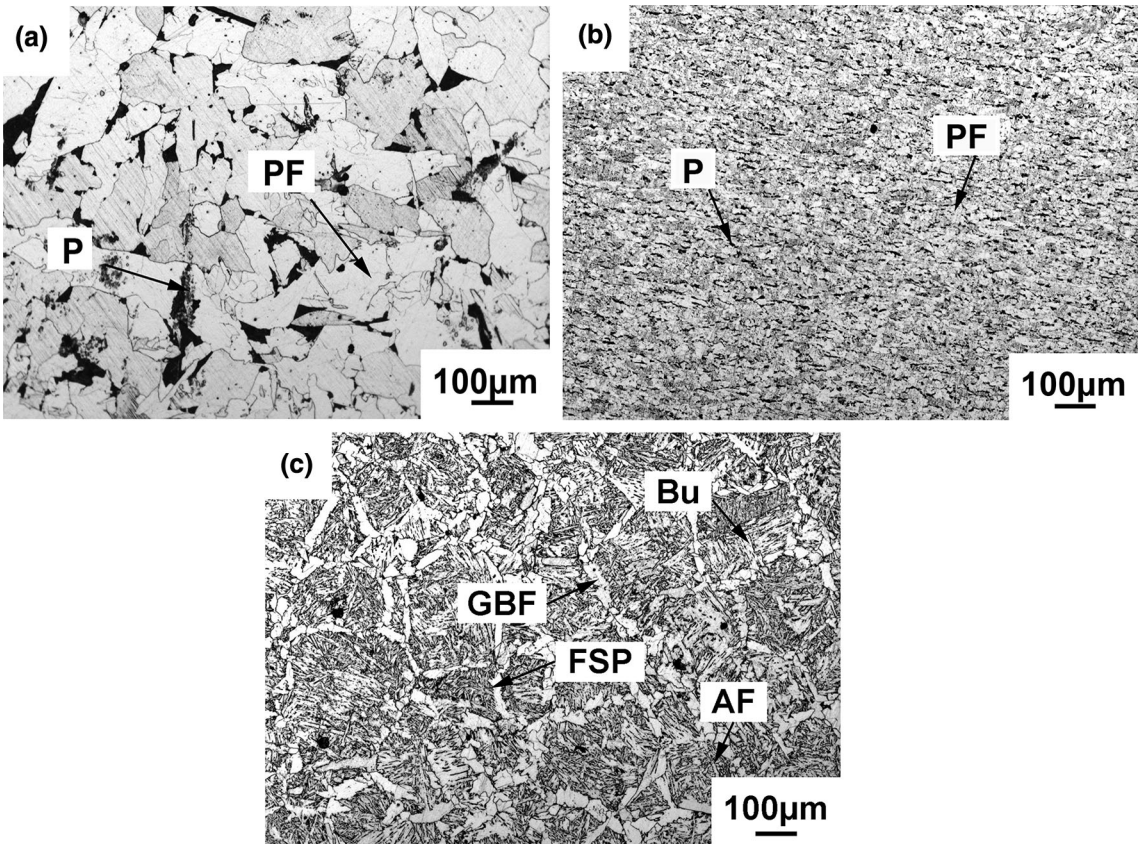

Fig. 6—Optical micrographs in (*a*) as-cast, (*b*) as-rolled, and (*c*) as-welded EH36 samples (*GBF* grain boundary ferrite, *FSP* ferrite side plate, *Bu* upper bainite, *AF* acicular ferrite, *P* pearlite, *PF* polygonal ferrite).

grew inward from the crucible wall and the prior austenite grains in the columnar dendrite zone display coarse columnar, showing a decrease of interdendritic spacing. Furthermore, Holappa *et al.*[24] suggested that Mn and S are enriched in the interdendritic melt. Therefore, the decrease of interdendritic spacing resulting from Mg addition increases the segregation of Mn and S in the interdendritic melt to promote the massive precipitation of MnS. The shape of individual MnS is rod like as shown in Figure 4(a) whose sizes are usually about 1 μm, beyond that polygonal MnS also exist whose sizes are usually between 0.1 and 0.5 μm. The result is in agreement with the report of Kimura *et al.*[25] They also demonstrated that in low-carbon Mg-killed steel, rod-like MnS precipitated at the nucleation sites of MgO or MnO-TiO_x inclusions in γ-Fe in the temperature range between 1500 K and 1200 K, while polygonal MnS precipitated in α-Fe at 1100 K just after the $\gamma \rightarrow \alpha$ transformation and their size was smaller than that of rod-like MnS. After TMCP and welding thermal simulation, the number of individual MnS decreases drastically. In the process of heating, the solubility of Mn and S increases[25] and diffuses in the steel. A larger interfacial area of coarser inclusion may facilitate MnS multiple nucleation on the surface.[26] Moreover, Hou *et al.*[27] reported that Ti and Mg-containing inclusions are effective to partition of Mn atom into oxides *via* first principle calculation. It is thus inferred that individual MnS in rolled and welded samples diffuse and precipitate on the surface of complex Ti-Al-Mg-O oxides.

B. *Effect of Mg Addition on Inclusions and Microstructure*

The inclusions in steel vary with the addition of Mg, which has strong ability of deoxidation. It can be seen from Figure 4 that Ti-Al-Mg-O oxides are generated and MnS precipitates on the surface of them in EH36-Mg. The dominant complex oxides are MgO-Al_2O_3 with a bundling structure and TiO_x on the outer layer as shown in Figure 8, which is in agreement with the phase relations in Al_2O_3-TiO_x-MgO system calculated by Park *et al.*[28]

Based on chemistry, inclusions could be classified as active or inert depending on their potential to promote AF nucleation. It is well known that various Ti-oxides are potent nuclei for the formation of AF.[29] Wu *et al.*[17] reported that AFs nucleated on the surface of MnS or at the junction between MnS and oxides. Those facts indicate that elements and elemental distribution in inclusions are related to AF nucleation. The structure of the inclusions in rolled and welded EH36-Mg is dominant multilayer as shown in Figures 8 and 9. The multilayer core oxides are composed of MgO-Al_2O_3 and TiO_x layer and MnS precipitates on the surface of the oxides. The results indicated that the above-mentioned inclusions were conducive to induce AF heterogeneous nucleation.

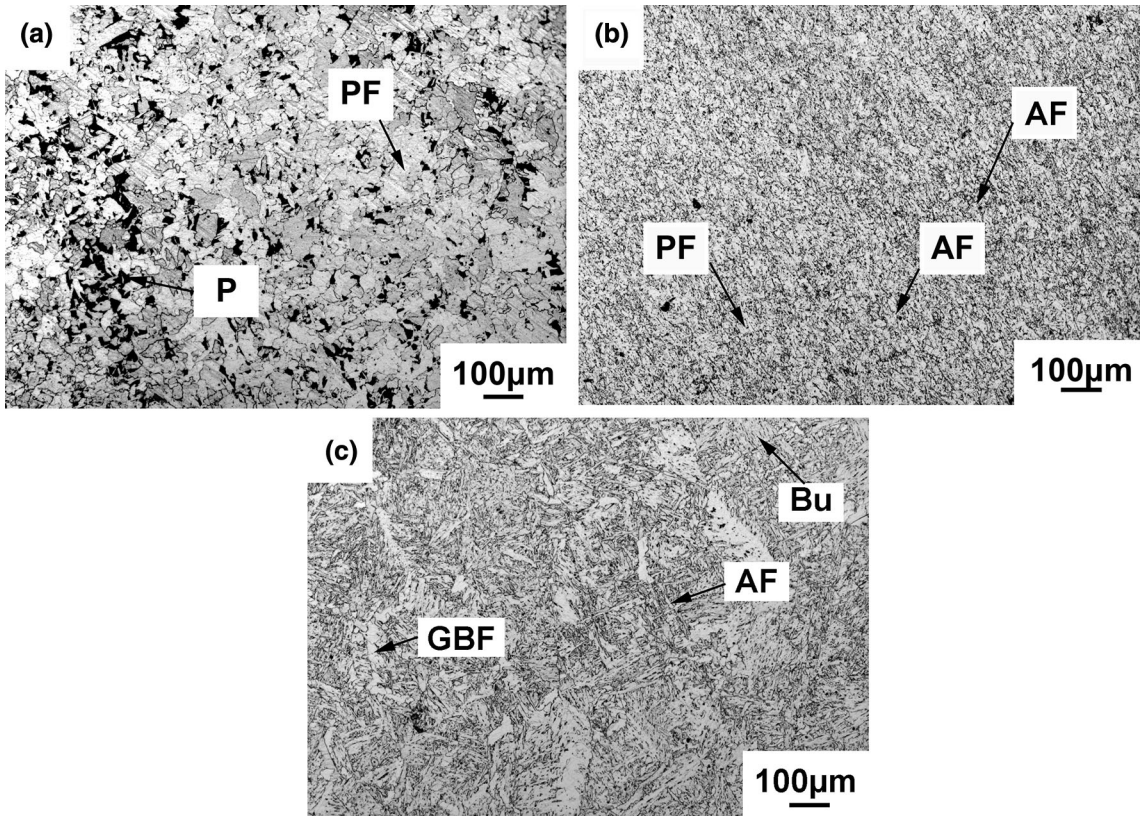

Fig. 7—Optical micrographs in (*a*) as-cast, (*b*) as-rolled, and (*c*) as-welded EH36-Mg samples (*GBF* grain boundary ferrite, *Bu* upper bainite, *AF* acicular ferrite, *P* pearlite, *PF* polygonal ferrite).

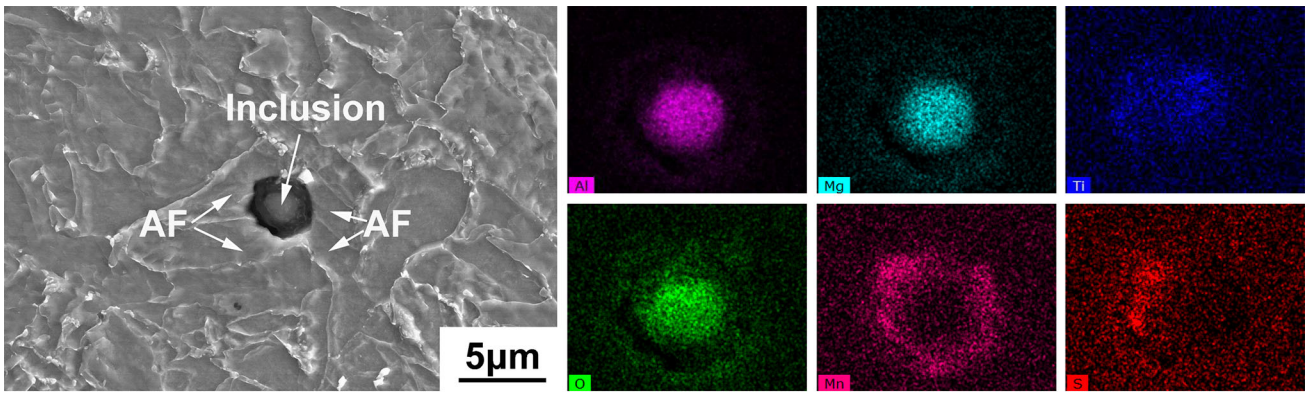

Fig. 8—SEM and EDS elemental mapping images of inclusion nucleating AF in the rolled EH36-Mg.

Beyond compositional considerations, size and number are important factors affecting ferrite nucleation. Lee *et al.*[30] reported that the probability of acicular ferrite nucleation on the surface of inclusions increased with inclusion size till 1 μm in low-carbon steel weld; when further increasing the size, the probability of ferrite nucleation did not continue to increase. Kim *et al.*[9] documented that the fraction of AF was proportional to the number density of inclusions which are smaller than 2 μm. Therefore, it is imperative to control the appropriate size of inclusions. With the addition of Mg, plenty of inclusions are generated, and the number density of inclusions increases from 108 to 220 N/mm^2 in the rolled sample. In the weld EH36-Mg sample, the inclusions with average size of 2.326 μm are more effective to the nucleation of AF.

The average austenite grain size is also one of the factors influencing AF nucleation, which are 247.64 and 145.24 μm for plain EH36 and EH36-Mg after welding thermal simulation, respectively. It could be found that in the welded samples, Mg addition effectively pins the grain boundary and promotes nucleation of AF as shown in Figure 9. When the temperature of thermal cycle is 1673 K (1400 °C), a larger number of fine pinning particles such as TiN grow up and coarsen[31] or dissolve in austenite, and lose the ability to pinning the

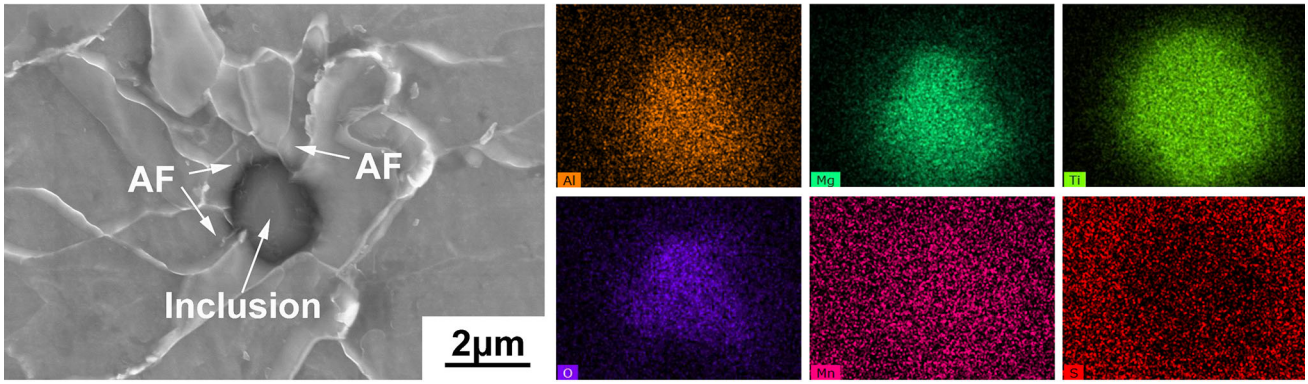

Fig. 9—SEM and EDS elemental mapping images of inclusion nucleating AF in the welded EH36-Mg.

Table II. The Result of Tensile Test in EH36 and EH36-Mg Samples

Samples	Yield Strength/MPa			Mean/MPa	Tensile Strength/MPa			Mean/MPa
As-cast EH36	241	239	235	238	382	381	378	380
Rolled EH36	391	386	394	390	488	491	489	489
As-cast EH36-Mg	289	261	241	264	411	423	400	411
Rolled EH36-Mg	415	424	406	415	537	536	520	531

Table III. The Results of Charpy Impact Test in Rolled EH36 and EH36-Mg Samples

Samples	Impact Toughness/J			Mean/J
Rolled EH36	280	254	262	265
Rolled EH36-Mg	327	295	345	322

migration of austenite grain boundaries which generally leads to the growth of grains.

The grain size could be predicted by utilizing inclusion size and the spatial distribution between inclusions based on Zener's model (Eq. [1]),[32] where grain size is predicted by the inclusion's ability to pin grain boundaries by exerting a pulling force.

$$R = \beta \frac{r}{f_V}, \qquad [1]$$

where R is the radius of a grain, r is the radius of the pinning inclusion, f_V is the volume fraction of second phase particles, β is a constant depending on the geometry and force balance.

According to Eq. [1], smaller particles and the volume fraction of the particles in steel will present stronger pinning effect of the particles on grains. A large number of Mg-containing inclusions in EH36-Mg could inhibit the growth of austenite at high temperature and induce interlocking AF structure nucleation.

V. CONCLUSIONS

In this study, characteristics of inclusions in plain EH36 and EH36-Mg shipbuilding steel have been systematically investigated in terms of inclusions' behavior and microstructure in the as-cast slabs, rolled plates, and simulated heat-affected zones, respectively. The following conclusions can be drawn.

1. In the as-cast EH36 sample, the inclusions are mainly composed of Al-Ca-S-O-(Mn) complex oxides and MnS precipitates. The size of inclusions mainly lies in the range of 1.0 to 2.0 μm. After rolling, the composition of inclusions does not undergo appreciable changes, while the average size of inclusions increases. After welding thermal simulation, the number of fine inclusions less than 1 μm decreases significantly. The microstructure in both as-cast and rolled sampled are composed of PF and P, while in the welded sample, the microstructure is composed of dominant GBF, FSP, and Bu.
2. In the as-cast EH36-Mg samples, a large amount of individually fine MnS precipitate and Ti-Al-Mg-O-(Mn-S) complex inclusions are generated. Comparing with plain EH36, those fine inclusions refine the microstructure significantly leading to improve the strength of steel. After rolling, individual MnS precipitation decreases, and AF nucleates on the surface of inclusions, which improves strength and impact toughness. After welding thermal simulation experiment, the inclusions in EH36-Mg are almost multilayer

or mosaic structure, consisting of Ti-Al-Mg-O complex oxides in the core and MnS on the surface. With Mg addition, the area fraction of AF in welded sample increases, while that of GBF, FSP, and Bu decreases significantly, and the growth of austenite grains is inhibited.

ACKNOWLEDGMENTS

The authors feel immensely grateful to the enabling financial support from National Natural Science Foundation of China (51622401 and 51628402), National Key Research and Development Program of China (2016YFB0300602), and Global Talents Recruitment Program endowed by the Chinese Government. We would also like to thank the support from Research Fund for Central Universities (N150205001), Key Laboratory of Nuclear Materials and Safety Assessment, Institute of Metal Research, Chinese Academy of Sciences (2015KF04), and State Key Laboratory of Advanced Welding and Joining, Harbin Institute of Technology (AWJ-16-Z04).

REFERENCES

1. W.M. Garrison and A.L. Wojcieszynski: *Mater. Sci. Eng., A*, 2007, vol. 464, pp. 321–29.
2. G.M. Faulring and S. Ramalingam: *Metall. Trans. A*, 1979, vol. 10, pp. 1781–88.
3. S. Mizoguchi, *The 19th Steelmaking Committee of the JSPS* 1999.
4. A. Kojima, K.-I. Yoshii, T. Hada, O. Saeki, K. Ichikawa, Y. Yoshida, Y. Shimura and K. Azuma, *Nippon Steel Tech. Rep*. 2004, pp. 33–37.
5. S. Suzuki, K. Ichimiya, and T. Akita: *JFE Tech. Rep*., 2005, vol. 5, pp. 24–29.
6. B.C. Kim, S. Lee, N.J. Kim, and D.Y. Lee: *Metall. Trans. A*, 1991, vol. 22, pp. 139–49.
7. C. Wang, R.D.K. Misra, M.H. Shi, P.Y. Zhang, Z.D. Wang, F.X. Zhu, and G.D. Wang: *Mater. Sci. Eng., A*, 2014, vol. 594, pp. 218–28.
8. H. Suito, A.V. Karasev, M. Hamada, R. Inoue, and K. Nakajima: *ISIJ Int*., 2011, vol. 51, pp. 1151–62.
9. B. Kim, S. Uhm, C. Lee, J. Lee, and Y. An: *J. Eng. Mater. Technol*., 2005, vol. 127, pp. 204–13.
10. D. Edmonds and R. Cochrane: *Metall. Trans. A*, 1990, vol. 21, pp. 1527–40.
11. J.H. Shim, Y.J. Oh, J.Y. Suh, Y.W. Cho, J.D. Shim, J.S. Byun, and D.N. Lee: *Acta Mater*., 2001, vol. 49, pp. 2115–22.
12. J. Lee and Y. Pan: *Mater. Sci. Eng., A*, 1991, vol. 136, pp. 109–19.
13. S. Ogibayashi: *Nippon Steel Tech. Rep*., 1994, vol. 61, pp. 70–76.
14. Z.T. Ma and D. Janke: *Acta Metall*., 1998, vol. 22, pp. 79–86.
15. L. Xu, J. Yang, R. Wang, Y. Wang, and W. Wang: *Metall. Mater. Trans. A*, 2016, vol. 47A, pp. 3354–64.
16. Z. Kai, Y. Jian, W. Ruizhi, and Y. Zhenguo: *J. Iron Steel Res. Int*., 2011, vol. 18, pp. 60–64.
17. Z. Wu, W. Zheng, G. Li, H. Matsuura, and F. Tsukihashi: *Metall. Mater. Trans. B*, 2015, vol. 46B, pp. 1226–41.
18. S. Wang, C. Chiang, and S. Chan: *Mater. Sci. Eng., A*, 2003, vol. 344, pp. 288–95.
19. Y. Wang, S. Sridhar, and M. Valdez: *Metall. Mater. Trans. B*, 2002, vol. 33B, pp. 625–32.
20. C. Feng, C. Yang, S. Hang, Y. Zhang, and X. Zhou: *J. Iron Steel Res. Int*., 2009, vol. 16, pp. 69–74.
21. H. Ohta and H. Suito: *ISIJ Int*., 2006, vol. 46, pp. 14–21.
22. K. Mukunthan, L. Strezov, R. Mahapatra and W. Blejde: in *The Brimacombe Memorial Symposium Proceedings*, 2000, pp 421–37.
23. K. Sakata and H. Suito: *Metall. Mater. Trans. A*, 2000, vol. 31A, pp. 1213–23.
24. L. Holappa, M. Hämäläinen, M. Liukkonen, and M. Lind: *Ironmaking Steelmaking*, 2003, vol. 30, pp. 111–15.
25. S. Kimura, K. Nakajima, S. Mizoguchi, and H. Hasegawa: *Metall. Mater. Trans. A*, 2002, vol. 33A, pp. 427–36.
26. H.-S. Kim, H.-G. Lee, and K.-S. Oh: *ISIJ Int*., 2002, vol. 42, pp. 1404–11.
27. Y. Hou, W. Zheng, Z. Wu, G. Li, N. Moelans, M. Guo, and B.S. Khan: *Acta Mater*., 2016, vol. 118, pp. 8–16.
28. S.-C. Park, I.-H. Jung, K.-S. Oh, and H.-G. Lee: *ISIJ Int*., 2004, vol. 44, pp. 1016–23.
29. J.-S. Byun, J.-H. Shim, Y. Cho, and D. Lee: *Acta Mater*., 2003, vol. 51, pp. 1593–1606.
30. T.K. Lee, H.J. Kim, B.Y. Kang, and S.K. Hwang: *ISIJ Int*., 2000, vol. 40, pp. 1260–68.
31. J. Moon, C. Lee, S. Uhm, and J. Lee: *Acta Mater*., 2006, vol. 54, pp. 1053–61.
32. C. Zener: *J. Appl. Phys*., 1949, vol. 20, pp. 950–53.